Applied Energy 269 (2020) 115104

Contents lists available at ScienceDirect

Applied Energy

journal homepage: www.elsevier.com/locate/apenergy

Parameter sensitivity analysis of electrochemical model-based battery management systems for lithium-ion batteries

Weihan Li[a,b,*], Decheng Cao[a], Dominik Jöst[a,b], Florian Ringbeck[a,b], Matthias Kuipers[a,b], Fabian Frie[a,b], Dirk Uwe Sauer[a,c,b,d]

[a] Chair for Electrochemical Energy Conversion and Storage Systems, Institute for Power Electronics and Electrical Drives (ISEA), RWTH Aachen University, Jaegerstrasse 17/19, 52066 Aachen, Germany
[b] Juelich Aachen Research Alliance, JARA-Energy, Germany
[c] Institute for Power Generation and Storage Systems (PGS) E.ON ERC, RWTH Aachen University, Germany
[d] Helmholtz Institute Münster (HI MS), IEK-12, Forschungszentrum Jülich, Germany

HIGHLIGHTS

- Comprehensive benchmarking of parameters for the lithium-ion electrochemical model.
- Parameter sensitivity analysis with different constant-current charging processes.
- Parameter sensitivity analysis under a real-world driving load of electric vehicles.
- Influence analysis of current rate and depth of discharge on parameter sensitivity.
- Parameter sensitivity rankings for functionalities in battery management systems.

GRAPHICAL ABSTRACT

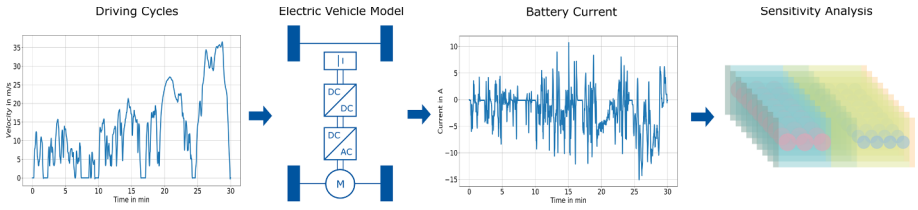

ARTICLE INFO

Keywords:
Battery
Lithium-ion
Parameter sensitivity
Electrochemical model
Battery management
Electric vehicles

ABSTRACT

Accurate identification of physical parameters of a lithium-ion electrochemical model is of critical importance for next-generation battery management systems. The complexity of the electrochemical model increases the difficulty of the identification process, and hence the analysis of parameter identifiability is the cornerstone for accurate parameter identification. The overarching goal of this paper is to analyze the parameter sensitivity of an electrochemical model under both the charging process and real-world driving cycles. The boundaries for the sensitivity analysis of 26 physical parameters are determined with a systematic benchmarking of published parameters for lithium Nickel-Manganese-Cobalt-Oxide/graphite cells. In particular, the sensitivity of the parameters is analyzed not only for terminal voltage but also for essential states in an electrochemical model-based battery management system, e.g., cathode bulk state of charge, cathode surface state of charge and anode potential. The sensitivity matrices of the parameters under different C-rates and depth of discharge regions clearly show their different influences on capacity-related parameters and other parameters. Furthermore, the rankings of the normalized parameter sensitivity index provide us the identifiability of the parameters, as well as the influence of parameter inaccuracy on the main functionalities in an electrochemical model-based battery management system.

* Corresponding author at: Chair for Electrochemical Energy Conversion and Storage Systems, Institute for Power Electronics and Electrical Drives (ISEA), RWTH Aachen University, Jaegerstrasse 17/19, 52066 Aachen, Germany.
E-mail addresses: batteries@isea.rwth-aachen.de, weihan.li@isea.rwth-aachen.de (W. Li).

https://doi.org/10.1016/j.apenergy.2020.115104
Received 4 February 2020; Received in revised form 15 April 2020; Accepted 26 April 2020
Available online 16 May 2020

1. Introduction

Due to their outstanding properties, such as high energy density, high reliability, and low self-discharge rate, lithium-ion batteries (LIBs) are becoming the dominating power source candidate for electric vehicles (EV). To guarantee a safe and reliable operation of LIBs, we need a battery management system (BMS), which is composed of software and hardware [1]. The state-of-the-art BMS is developed based on an equivalent circuit model (ECM) of the battery, which provides simple battery states and parameters, e.g., open-circuit voltage and ohmic resistance. Based on this lumped model, battery diagnostic algorithms can be further developed to estimate the battery states and parameters. Due to the simple model structure, low computation burden, and easy parameterization process, the ECM has been pushed into wide applications in industry. However, the model simplicity also restricts ECM to show more physical meaning in its states and parameters. Moreover, due to the limited estimation capabilities of ECMs, the battery operation strategy has to be designed based on simple safety constraints, e.g., maximum and minimum voltage and current, which are conservative, especially at high currents. Furthermore, the voltage and current limits may not guarantee safety as the battery ages, which leads to potentially dangerous operation.

With the emergence of new demands in modern battery systems for autonomous driving vehicles, e.g., ultra-fast charging, precise lifetime prediction and further reduction of battery weight and cost, a smarter and more intelligent BMS with advanced battery diagnostic algorithms is needed. To this end, instead of using the lumped ECM, the researchers use electrochemical models as the basic model to develop new battery diagnostic frameworks. The diagnostics using electrochemical models are able to estimate the spatially distributed essential states of LIBs, e.g., lithium-ion concentration and potential in electrode and electrolyte. As the onset of most damaging effects during ultra-fast charging and high-dynamic operations is defined by these states, safer operational constraints can be imposed [2]. Compared with the ECM, which has parameters that are less physically relevant, an electrochemical model contains a large number of parameters with a physical meaning. This provides the opportunity for a deep understanding of the aging mechanisms of the LIB using electrochemical models. However, new challenges in identifying the physical parameters fast and accurately for the BMS are appearing in the vision of the engineers and researchers. Ecker et al. [3,4] introduced a complete experimental process for the parameterization of an electrochemical model for a 7.5 Ah Kokam cell and validated the measured parameters with experiments. In [5,6], both the electrochemical and thermal parameters for a 28 Ah high power cell were measured and validated experimentally. In order to further improve the parameter accuracy, Tang et al. [7] presented a systematic method combining experimental and computational approaches for key parameters acquisition in 4.35 V $LiCoO_2$ batteries. However, the identification approaches are still not fast and accurate enough for the application of the electrochemical models in BMSs.

Before the design of a fast parameter identification framework for the electrochemical model-based BMS, the identifiability of the parameters in an electrochemical model should be studied under various operational conditions. The identifiability of the parameters can be examined with parameter sensitivity analysis, i.e., the analysis for the variance of the model output due to the variance of the parameter itself. Parameter sensitivity analysis has already been used in the lithium-ion electrochemical model for determining the identifiability of the model parameters [8–12].

Schmidt et al. [8] and Forman et al. [9] used the Fisher information matrix (FIM) to study parameter sensitivity by employing the terminal voltage as model output. Forman et al. have concluded some unidentifiable parameters which do not affect the terminal voltage of the electrochemical model. To determine the identifiability, Schmidt et al. used the least eigenvalue of FIM and Forman et al. used a threshold value for the minimum condition number of FIM. Although FIM offers a minimum variance bound and confidence interval of the parameters, the calculation process of FIM is very complex for high-order electrochemical models.

Without calculating the FIM, Zhang et al. [10] carried out a local sensitivity analysis for 30 parameters of their electrochemical model for $LiFePO_4$ batteries using a simulation-based method. Furthermore, the surface temperature of the battery has been used as one of the outputs of the model for the parameter sensitivity analysis. Based on this work, Edouard et al. [11] extended the same analysis method to another simplified electrochemical and thermal model. A parameter sensitivity matrix for the terminal voltage and cell skin temperature has been studied under various operating conditions. Ghaznavi et al. [12] performed a sensitivity analysis of the electronic conductivity of the cathode for a lithium-sulfur battery under discharging current. The nonlinear response of the electrochemical model to the parameter variation has been observed. It is worth noting that the determination of value ranges of the physical parameters, which influences the parameter sensitivity, has not been conducted based on a wide literature review and experiments in the above pioneering work. Moreover, they only used the deviation of the terminal voltage and cell temperature under constant discharging current profile as the sensitivity index (SI) of the parameters. The sensitivity of the parameters in an electrochemical model under the real-world operation load of EVs is still not clear. In addition, the influence of the inaccuracy of the insensitive parameters on the main BMS functionalities is also missing.

Aiming at bridging the aforementioned research gap, this paper benchmarks the value ranges of 26 physical parameters for LIBs with Nickel-Manganese-Cobalt-Oxide (NMC) as cathode material and graphite as anode material. Based on the benchmarking results, we analyze the sensitivity of the electrochemical model to cell parameters not only under constant C-rate charging but also under real-world driving cycles. Furthermore, the relationship between the parameter sensitivity and C-rate is analyzed considering the sensitivity variance among depth of discharge (DOD) regions. For the first time, the sensitivity of the parameters is looked into for not only terminal voltage, but also essential states in an electrochemical model-based BMS, e.g., cathode bulk state of charge (SOC), cathode surface SOC, and anode potential. This work is the first step of broader research on the development of a fast parameter identification framework for lithium-ion electrochemical models.

The remainder of the paper is organized as follows: we begin in Section 2 by introducing the lithium-ion electrochemical model. The parameter benchmarking for lithium-NMC-graphite cells is introduced in Section 3 and the sensitivity analysis methods are presented in Section 4. In Section 5, the sensitivity analysis results are presented and the inspiration for the identification of parameters in electrochemical models is discussed. The conclusions and future works are drawn in Section 6.

2. Lithium-ion electrochemical model

The Pseudo-2D (P2D) model developed by Doyle et al. [13] based on porous electrode theory is the most popular electrochemical model describing the solid and electrolyte dynamics of LIBs. Based on the diffusion of lithium-ions in electrodes and electrolyte, the spatial and temporal distribution of lithium-ion concentrations and potentials in the battery can be derived, as depicted in Fig. 1. The governing nonlinear partial differential algebraic equations (PDAEs) of the P2D model are summarized in this section. The readers are referred to [2] for further derivation details.

With the assumption of charge neutrality within the solid spherical particles with radius R_p, the dynamics of the lithium-ion concentration

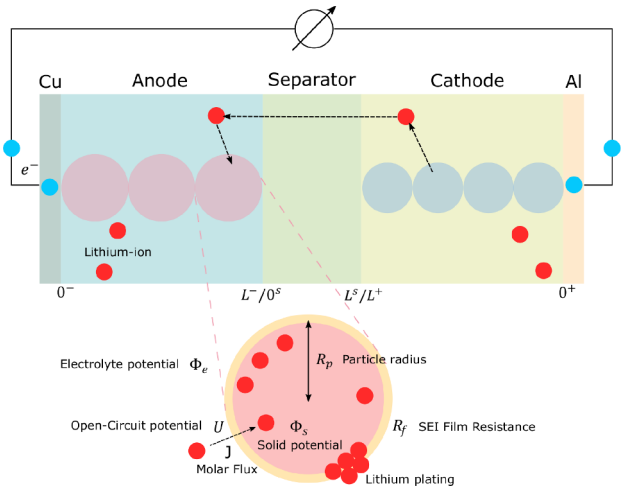

Fig. 1. Schematic of the electrochemical model for LIBs.

in solid active material can be described by Fick's law in r-direction as

$$\frac{\partial c_s(x,\,r,\,t)}{\partial t} = \frac{1}{r^2}\frac{\partial}{\partial r}\left(r^2 D_s \frac{\partial c_s(x,\,r,\,t)}{\partial r}\right) \tag{1}$$

where $c_s(x,\,r,\,t)$ denotes the lithium-ion concentration in electrodes at spatial coordinate x and radial coordinate r, D_s is the solid diffusion coefficient of lithium-ions. The dependency of D_s on SOC is neglected in this work. The boundary conditions of Eq. (1) are given by

$$\left.\frac{\partial c_s(x,\,r,\,t)}{\partial r}\right|_{r=0} = 0 \tag{2}$$

$$\left.\frac{\partial c_s(x,\,r,\,t)}{\partial r}\right|_{r=R_p} = -\frac{j(x,\,t)}{D_s} \tag{3}$$

with $j(x,\,t)$ as the molar flux of lithium-ions on the particle surface.

Considering the changes of lithium-ions in electrolyte due to the concentration difference-induced diffusion and electrolyte current, the electrolyte dynamics can be defined by

$$\frac{\partial c_e(x,\,t)}{\partial t} = \frac{\partial}{\partial x}\left(D_{e,eff}\frac{\partial c_e(x,\,t)}{\partial x}\right) + \frac{1-t_0^+}{\varepsilon_e F}\frac{\partial i_e(x,\,t)}{\partial x} \tag{4}$$

where $c_e(x,\,t)$ and $i_e(x,\,t)$ denote the lithium-ion concentration and the current in the electrolyte, $D_{e,eff}$ is the effective electrolyte diffusion coefficient, t_0^+ is the transference number for the cations, ε_e is the volume fraction of the electrolyte and F is the Faraday's constant. The spatial change of $i_e(x,\,t)$ can be further described by

$$\frac{\partial i_e(x,\,t)}{\partial x} = aFj(x,\,t) \tag{5}$$

where a is the specific interfacial area. The boundary conditions at current collectors and borders between electrodes and separator are as follows,

$$\left.\frac{\partial c_e(x,\,t)}{\partial x}\right|_{x=0^-} = \left.\frac{\partial c_e(x,\,t)}{\partial x}\right|_{x=0^+} = 0 \tag{6}$$

$$\left.\varepsilon_e^- D_{e,eff}\frac{\partial c_e(x,\,t)}{\partial x}\right|_{x=L^-} = \left.\varepsilon_e^s D_{e,eff}\frac{\partial c_e(x,\,t)}{\partial x}\right|_{x=0^s} \tag{7}$$

$$\left.\varepsilon_e^s D_{e,eff}\frac{\partial c_e(x,\,t)}{\partial x}\right|_{x=L^s} = \left.\varepsilon_e^+ D_{e,eff}\frac{\partial c_e(x,\,t)}{\partial x}\right|_{x=L^+} \tag{8}$$

$$c_e(L^-,\,t) = c_e(0^s,\,t) \tag{9}$$

$$c_e(L^s,\,t) = c_e(L^+,\,t) \tag{10}$$

where 0^- and 0^+ correspond to the boundaries between current collectors and electrodes, $L^-/0^s$ and L^s/L^+ correspond to the boundaries between separator and electrodes, as shown in Fig. 1.

The variation of the solid electrode potential, $\Phi_s(x,\,t)$, can be expressed by Ohm's law as

$$\frac{\partial}{\partial x}\left(\sigma_s \varepsilon_s \frac{\partial \Phi_s(x,\,t)}{\partial x}\right) = aFj(x,\,t) \tag{11}$$

where σ_s is the electrode conductivity and ε_s is the volume fraction of the active material. Furthermore, the spatiotemporal dynamics of the electrolyte potential, $\Phi_e(x,\,t)$, is defined as

$$\frac{\partial \Phi_e(x,\,t)}{\partial x} = -\frac{i_e(x,\,t)}{\sigma_{e,\text{eff}}} + \frac{2RT}{F}(1-t_0^+)\left(1+\frac{\partial ln f_+}{\partial ln c_e(x,\,t)}\right)\frac{\partial ln c_e(x,\,t)}{\partial x} \tag{12}$$

where $\sigma_{e,\text{eff}}$ is the effective electrolyte conductivity, R is the universal gas constant, T is the temperature of the cell, and f_+ is the activity coefficient in the electrolyte. The overpotential of lithium-ion intercalation, $\eta(x,\,t)$, is given by

$$\eta(x,\,t) = \Phi_s(x,\,t) - \Phi_e(x,\,t) - U\left(\frac{c_{ss}(x,\,t)}{c_{s,\max}}\right) - FR_f j(x,\,t) \tag{13}$$

where $c_{s,\max}$ is the maximum lithium-ion concentration of the electrode and R_f is the film resistance between electrode and electrolyte, as depicted in Fig. 1. The electrode open-circuit potential, U, depends on the lithium-ion concentration on the surface of electrode particles, $c_{ss}(x,\,t)$, which can be expressed by high-order polynomials.

Furthermore, the relationship between the molar flux, $j(x,\,t)$, and the intercalation overpotential, $\eta(x,\,t)$, is given by the Butler-Volmer kinetics

$$j(x,\,t) = \frac{i_0(x,\,t)}{F}\left[\exp\left(\frac{(1-\alpha)F}{RT}\eta(x,\,t)\right) - \exp\left(-\frac{\alpha F}{RT}\eta(x,\,t)\right)\right] \tag{14}$$

where $\alpha = 0.5$ is the charge transfer coefficient and the exchange current density, $i_0(x,\,t)$, is defined by

$$i_0(x,\,t) = \kappa c_e^{1-\alpha}(c_{s,\max} - c_{ss}(x,\,t))^{1-\alpha} c_{ss}(x,\,t)^{\alpha}. \tag{15}$$

where κ is the reaction rate coefficient.

In summary, the solid and electrolyte dynamics of LIBs are described with Eqs. (1)–(15). However, the evaluation of the P2D model requires a large computation effort because of the coupled PDAEs, which makes it extremely hard to be applied in an embedded BMS. To facilitate computation simplicity, a reduced-order electrochemical model with 10 discretization nodes in each domain for LIBs was developed in this work with the finite-difference method [14] in micro-scale and the finite-volume method [15] in macro-scale. The readers are referred to [16] for a structural understanding of model order reduction techniques for electrochemical models.

3. Parameter benchmarking for lithium-NMC-graphite cells

In contrast to ECM, electrochemical models consist of a large number of physical parameters, the experimental identification process of which is complicated, expensive and time-consuming [3]. One of our goals is to develop a fast parameter identification framework for electrochemical models which is suitable for not only a specific cell but also all the cells with the same chemistry. As summarized in Table 1, the focused 26 parameters in this work were grouped into four categories: geometric parameters, transport parameters, kinetic parameters, and concentration parameters. The analysis of the polynomial fitting

Table 1
List of parameter benchmarking values for lithium-NMC-graphite cells and value ranges for sensitivity analysis.

Category	Parameter	Unit	Description	Benchmarking	Boundaries
Geometric parameters	L^+	μm	Cathode thickness	74[17], 36.4[18], 78[19], 47[20], 70[21], 79[22], 60[23], 54.5[3]	35–79 μm
	L^s	μm	Separator thickness	25[17,18,22,24], 20[19,20,23], 19[3], 10–30[25]	10–30 μm
	L^-	μm	Anode thickness	62[17], 50[18], 81[19], 52[20], 63[21], 67[22], 90[23], 73.7[3]	35–79 μm
	A	m^2	Electrode surface area	Experimental measurement of Kokam SLPB 75106100 cell	0.378–0.395 m^2
	ε_s^+	–	Cathode active material volume fraction	0.38[17], 0.5[21], 0.375[22], 0.428[3]	0.35–0.5
	ε_s^-	–	Anode active material volume fraction	0.45[17], 0.42[21], 0.419[22], 0.4[3]	0.4–0.5
	ε_e^+	–	Cathode electrolyte volume fraction	0.45[17], 0.330[18], 0.281[19], 0.27[20], 0.35[21], 0.33[23], 0.296[3], 0.3[26]	0.27–0.45
	ε_e^s	–	Separator electrolyte volume fraction	0.5[17], 0.5[18,22,23], 0.4[26], 0.46[19], 0.4[20], 0.508[3]	0.4–0.55
	ε_e^-	–	Anode electrolyte volume fraction	0.5[17], 0.332[18], 0.264[19], 0.34[20], 0.33[21,23], 0.329[3], 0.3[26]	0.26–0.5
	R_p^+	μm	Cathode particle radius	5[19,20,24,26], 1.2[21], 7[22], 6.49[3]	1–11 μm
	R_p^-	μm	Anode particle radius	10[19,20],5[24,26], 11[22], 8.7[3]	1–11 μm
Transport parameters	D_s^+	$m^2\ s^{-1}$	Cathode solid diffusion coefficient	$3{\cdot}10^{-14}$[17,19,20], $3.97{\cdot}10^{-14}$[23], $2{\cdot}10^{-14}$[24,26], $8{\cdot}10^{-14}$[27]	$1{\cdot}10^{-14}$ - $1{\cdot}10^{-13}$ $m^2\ s^{-1}$
	D_s^-	$m^2\ s^{-1}$	Anode solid diffusion coefficient	$3{\cdot}10^{-14}$[17], $1.75{\cdot}10^{-14}$[19], $2{\cdot}10^{-14}$[23], $1.54{\cdot}10^{-14}$[24], $1.4{\cdot}10^{-14}$[26], $8.8{\cdot}10^{-14}$[27]	$1{\cdot}10^{-14}$ - $1{\cdot}10^{-13}$ $m^2\ s^{-1}$
	D_e	$m^2\ s^{-1}$	Electrolyte diffusion coefficient	$2.6{\cdot}10^{-10}$[18,23], $2.4{\cdot}10^{-10}$[3], $1.5{\cdot}10^{-10}$ - $4.5{\cdot}10^{-10}$[28], $2{\cdot}10^{-10}$ - $4.5{\cdot}10^{-10}$[29]	$1.5{\cdot}10^{-10}$ - $4.5{\cdot}10^{-10}$ $m^2\ s^{-1}$
	b^+	–	Cathode Bruggeman coefficient	1.5[18,24]	1.3–1.7
	b^s	–	Separator Bruggeman coefficient	1.5[18,23,24,27]	1.3–1.7
	b^-	–	Anode Bruggeman coefficient	1.5[18,24]	1.3–1.7
	t_0^+	–	Transference number of lithium cation	0.38[17,26,27], 0.363[18,23], 0.26[3], 0.37–0.43[28], 0.25–0.4[30], 0.36–0.4[31]	0.25–0.43
	σ_s^+	μm	Cathode electrode conductivity	36–185[32]	36–185 μm
	σ_s^-	μm	Anode electrode conductivity	1 - $1{\cdot}10^4$[33]	1 - $1{\cdot}10^4$ μm
Kinetic parameters	κ^+	$m^{2.5}\ mol^{0.5}\ s$	Cathode reaction rate coefficient	$2{\cdot}10^{-11}$[17,21,22], $4.38{\cdot}10^{-11}$[20], $3.01{\cdot}10^{-11}$[3]	$1{\cdot}10^{-11}$ - $1{\cdot}10^{-10}$ $m^{2.5}\ mol^{0.5}\ s$
	κ^-	$m^{2.5}\ mol^{0.5}\ s$	Anode reaction rate coefficient	$2{\cdot}10^{-11}$[17,22], $1.63{\cdot}10^{-11}$[20], $1.45{\cdot}10^{-11}$[3]	$1{\cdot}10^{-11}$ - $2{\cdot}10^{-10}$ $m^{2.5}\ mol^{0.5}\ s$
	R_f	Ωm^2	Anode SEI film resistance	$1{\cdot}10^{-2}$[19], $3.5{\cdot}10^{-3}$[22], $1{\cdot}10^{-3}$[27]	$1{\cdot}10^{-3}$ - $1{\cdot}10^{-2}$ Ωm^2
Concentration parameters	$c_{s,\max}^+$	$mol\ m^{-3}$	Cathode maximum ionic concentration	$5.15{\cdot}10^4$[17], $4.9242{\cdot}10^4$[22], $4.858{\cdot}10^4$[3], $4.95{\cdot}10^4$[24,27], $5.183{\cdot}10^4$[26]	$4.8{\cdot}10^4$ - $5.2{\cdot}10^4$ $mol\ m^{-3}$
	$c_{s,\max}^-$	$mol\ m^{-3}$	Anode maximum ionic concentration	$3.137{\cdot}10^4$[17], $2.9862{\cdot}10^4$[22], $3.192{\cdot}10^4$[3], $3.09{\cdot}10^4$[24], $3.108{\cdot}10^4$[26], $3.0555{\cdot}10^4$[27]	$2.9{\cdot}10^4$ - $3.3{\cdot}10^4$ $mol\ m^{-3}$
	$c_{e,0}$	$mol\ m^{-3}$	Initial electrolyte concentration	$1{\cdot}10^3$[20,3], $1.2{\cdot}10^3$[24,18,26,19,27,23]	$1{\cdot}10^3$ - $1.2{\cdot}10^3$ $mol\ m^{-3}$

parameters in the functions of open-circuit potential[1,2] and effective electrolyte conductivity[3] is beyond the scope of this work.

- **Geometric parameters**
  There are 11 parameters classified as geometric parameters, which represent the geometric characteristics of the cells, e.g., compartment thicknesses, electrode surface area, active material volume fractions, electrolyte volume fraction and electrode particle radiuses.
- **Transport parameters**
  There are nine parameters classified as transport parameters, e.g., diffusion coefficients in electrodes and electrolyte, Bruggeman coefficients, transference number of lithium cation and electrode conductivities, describing the capability of the cell for the transport of particles, ions, and charges.
- **Kinetic parameters**
  The kinetic parameters represent the capability of the cell regarding charge transfer. Among all physical parameters, three parameters were categorized as kinetic parameters, e.g., reaction rate coefficient and SEI film resistance, according to the Butler-Volmer kinetics.
- **Concentration parameters**
  Apart from the physical parameters mentioned above, three parameters are representing the concentration levels of lithium-ions in electrodes and electrolytes. Concentration parameters include the maximum lithium concentration in cathode and anode material and the initial lithium concentration in the electrolyte.

Reasonable value ranges of the parameters are of critical importance for parameter sensitivity analysis and identification. Unlike the previous work, the value ranges of these 26 physical parameters were determined carefully for lithium-NMC-graphite cells according to more than 25 literature references and experiments, as shown in Table 1. The superscripts $+$, $-$, s of the parameters represent cathode, anode, and separator, respectively. Considering the wide application of lithium-NMC-graphite cells in the automotive industry, we choose NMC/graphite as the research focus in this work. The determination of parameter ranges for the cells with other materials, such as *LiFePO4/graphite*, is out of the scope of this work and will be investigated in the future. Based on the value ranges of parameters for lithium-NMC-graphite cells, sensitivity analysis of physical parameters will be introduced in the following sections.

4. Parameter sensitivity analysis

Each parameter of the electrochemical model has a specific influence with various levels of impact on the accuracy of the model output. A sensitivity analysis of all the 26 physical parameters under various conditions was carried out in this work to investigate the sensitivity of the parameters under both constant C-rate charging process and real-world vehicle operation load. In particular, the influences of the inaccuracy of the parameters on the functionalities of the electrochemical model-based BMS were studied for the first time.

4.1. Parameter sensitivity for electrochemical states in BMSs

In this work, the parameter sensitivity analysis was conducted not only on terminal voltage but also on essential states in an electrochemical model-based BMS to investigate the influence of parameter inaccuracy on the BMS functionalities. The physical description of these essential states and the related BMS functionalities will be introduced in detail as follows.

4.1.1. Terminal voltage

The terminal voltage of the cell can be calculated by

$$V(t) = \Phi_s(0^+, t) - \Phi_s(0^-, t) \tag{16}$$

where 0^+ and 0^- correspond to the boundaries between current collectors and electrodes, as shown in Fig. 1. As one of the measurable states of the battery, the terminal voltage is an important input for parameter identification algorithms in electrochemical model-based BMSs. Therefore, the sensitivity of the parameters related to the terminal voltage can provide us not only with the influence of parameter inaccuracy on battery modeling accuracy but also the parameter identifiability for data-based parameter identification methods in BMSs.

4.1.2. Cathode bulk SOC

The cathode bulk SOC of a cell can be expressed as

$$SOC^+(t) = \frac{1}{N_x^+}\sum_{i=1}^{N_x^+}\frac{\frac{\bar{c}_{s,i}^+(t)}{c_{s,\max}^+} - \theta_0^+}{\theta_{100}^+ - \theta_0^+} \tag{17}$$

where $\bar{c}_{s,i}^+(t)$ is the average lithium-ion concentration in i^{th} cathode particle, N_x^+ is the discretization number in cathode, θ_0^+ and θ_{100}^+ are the stoichiometry parameters of the cathode at 0% and 100% SOC. The bulk SOC represents roughly the average utilization of lithium-ions in the electrode, which is estimated in an electrochemical model-based BMS to yield the energy content stored in the battery pack, i.e., state of energy (SOE). According to our observability analysis, the bulk SOC in the cathode is more observable than that in anode because of the flatness of the anode open-circuit potential. Furthermore, deep delithiation of NMC cathode material makes the cathode unstable and accelerates the aging process, which should be avoided. Thus, cathode bulk SOC was chosen in this work as one electrochemical battery state for parameter sensitivity analysis.

4.1.3. Cathode surface SOC

The cathode surface SOC is described by

$$SOC_s^+(t) = \frac{1}{N_x^+}\sum_{i=1}^{N_x^+}\frac{\frac{c_{ss,i}^+(t)}{c_{s,max}^+} - \theta_0^+}{\theta_{100}^+ - \theta_0^+} \tag{18}$$

where $c_{ss,i}^+(t)$ denotes the lithium-ion concentration on the surface of the i^{th} cathode particle. In contrast to bulk SOC, the surface SOC represents the utilization of lithium-ions on the surface of the electrodes, strongly determining the instantaneous power output of the cell, which is usually used in an electrochemical model-based BMS as an important state for power prediction, i.e., state of power (SOP).

4.1.4. Anode potential

One of the highlights of an electrochemical model-based BMS is the ability to monitor the occurrence of the side reactions, such as lithium plating [34], which can age or even damage the cell. Lithium plating is directly related to negative lithium deposition overpotential, which presents a favorable condition for the formulation of lithium plating, as expressed by [35]

[1] Cathode open-circuit potential: $U^+ = 2.11 \times 10^{-6} + 110.52 \times (1-\theta) - 1361.72 \times (1-\theta)^2 + 9188.4 \times (1-\theta)^3 - 37148.01 \times (1-\theta)^4 + 94012.19 \times (1-\theta)^5 - 150327.14 \times (1-\theta)^6 + 147704.4 \times (1-\theta)^7 - 81484.34, \times (1-\theta)^8 + 19336.88 \times (1-\theta)^9 + 0.1 \times \exp(-57824.14\theta^{115})$
where $\theta = \frac{c_{ss}^+(x,t)}{c_{s,\max}^+}$.

[2] Anode open-circuit potential: $U^- = 0.14 + 0.75 \times \exp(-35.61\theta) - 0.02 \times \tanh\left(\frac{\theta-0.61}{0.02}\right) - 0.13 \times \tanh\left(\frac{\theta-0.32}{0.07}\right) - 0.12 \times \tanh\left(\frac{\theta-0.21}{0.09}\right) - 0.13 \times \tanh\left(\frac{\theta-0.45}{0.16}\right) - 0.12 \times \tanh\left(\frac{\theta-0.4}{0.16}\right) - 0.11 \times \tanh\left(\frac{\theta-0.43}{0.15}\right) - 0.15 \times \tanh\left(\frac{\theta-0.4}{0.1}\right) + 0.72 \times \tanh\left(\frac{\theta-0.37}{0.16}\right)$
where $\theta = \frac{c_{ss}^-(x,t)}{c_{s,\max}^-}$.

[3] Effective electrolyte conductivity: $\sigma_e = 0.1726 + 1.7919\cdot10^{-3}c_e - 1.2983\cdot10^{-6}c_e^2 + 2.6670\cdot10^{-10}c_e^3$.

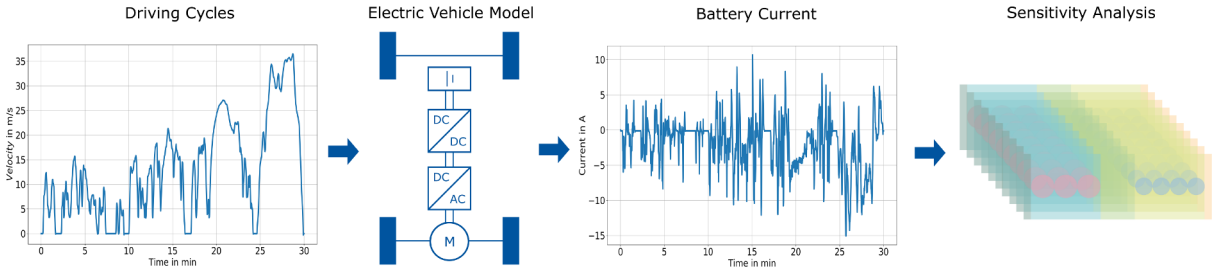

Fig. 2. Framework of parameter sensitivity analysis for the electrochemical model-based BMS under real-world driving cycles. An EV model [37] generates the current data of the battery based on the velocity data of the EV under WLTP driving cycles. The generated current data are then applied as input data to the reduced-order electrochemical model and the parameter value varies within its benchmarking range for the sensitivity analysis.

$$\begin{aligned}\eta_{Li}(x,t) &= \Phi_s(x,t) - \Phi_e(x,t) - U_{eq,Li}(x,t) - \frac{R_f}{a_s}(j(x,t) + j_{Li}(x,t))\\ \eta_{LiP}(x,t) &= \min(0, \eta_{Li}(x,t))\end{aligned} \tag{19}$$

where a_s, $U_{eq,Li}(x,t)$ and $j_{Li}(x,t)$ are the specific active area, equilibrium potential and molar flux for lithium plating, respectively. In this research, anode potential $\Phi(x,t) = \Phi_s(x,t) - \Phi_e(x,t)$ is used for simplification purpose considering that anode potential is a more conservative limitation than lithium plating overpotential. According to [2,35,36], lithium plating is possible when:

$$\Phi(x,t) = \Phi_s(x,t) - \Phi_e(x,t) < 0. \tag{20}$$

Thus, the parameter sensitivity for the anode potential $\Phi^-(t) = \Phi(L^-, t)$ was analyzed in this work, where L^- is the most critical location for lithium plating, as shown in Fig. 1.

4.2. Methodology

With the parameter range benchmarked in Section 3, the sensitivity of all the 26 parameters was analyzed individually by investigating the variability of the BMS states introduced in Section 4.1 against the variation of the corresponding parameters. In this work, One-At-a-Time (OAT) method [10] was applied to investigate the output variability against the variations of an input factor around a specific value. $N_s = 10$ value points of each parameter p were selected under discrete uniform distribution between its lower and upper boundary while all the rest parameters were remaining with the nominal value. The i^{th} value point p_i and the nominal value $\bar{p}$ of each parameter p can be described as,

$$p_i = p_l + (i-1)\frac{p_u - p_l}{N_s} \tag{21}$$

$$\bar{p} = \frac{p_l + p_u}{2} \tag{22}$$

where p_l and p_u are the lower and upper boundaries of the parameter p, respectively, as summarized in Table 1. For the parameters with boundaries in different order of magnitude, the value points and the nominal value were determined in logarithmic scale as follows,

$$\log p_i = \log p_l + (i-1)\frac{\log p_u - \log p_l}{N_s} \tag{23}$$

$$\log \bar{p} = \frac{\log p_l + \log p_u}{2}. \tag{24}$$

4.2.1. Parameter sensitivity under constant C-rate charging process

To analyze the sensitivity of the parameters, constant current constant voltage (CC-CV) charging profiles were first used as the input profiles for the proposed reduced-order electrochemical model in Section 2. Seven different C-rates of the charging current, e.g., 0.25 C, 0.5 C, 1 C, 2 C, 3 C, 4 C, and 5 C, were applied to investigate the relationship between parameter sensitivity and current magnitude, which contributes to the design of parameter identification scenarios.

As the dispersion of the states indicates the sensitivity of the parameter, the mean standard deviation of the analyzed state x_i at specific SOC point and C-rate was chosen as the sensitivity index (SI),

$$SI(SOC, C) = \sqrt{\frac{1}{N_s}\sum_{j=1}^{N_s}(x_{ij} - \bar{x}_i)^2} \tag{25}$$

where N_s is the number of value points in each parameter range and $\bar{x}_i$ is the average value of the states x_{ij}.

In order to investigate the relationship between the variance of parameter sensitivity and variance of SOC, the average sensitivity index (ASI) of the parameters at five DOD regions were calculated as follows,

$$ASI(0\% - 20\%, C) = \frac{1}{N_{DOD_5}}\sum_{j=1}^{N_{DOD_5}} SI(SOC, C) \tag{26}$$

$$ASI(20\% - 40\%, C) = \frac{1}{N_{DOD_4}}\sum_{j=1}^{N_{DOD_4}} SI(SOC, C) \tag{27}$$

$$ASI(40\% - 60\%, C) = \frac{1}{N_{DOD_3}}\sum_{j=1}^{N_{DOD_3}} SI(SOC, C) \tag{28}$$

$$ASI(60\% - 80\%, C) = \frac{1}{N_{DOD_2}}\sum_{j=1}^{N_{DOD_2}} SI(SOC, C) \tag{29}$$

$$ASI(80\% - 100\%, C) = \frac{1}{N_{DOD_1}}\sum_{j=1}^{N_{DOD_1}} SI(SOC, C) \tag{30}$$

where N_{DOD_i} is the number of data points in i^{th} DOD region before the reach of the cut-off voltage. If the terminal voltage of the battery arrives at the cut-off voltage before the DOD_1 region,

$$ASI(80\% - 100\%, C) = ASI(60\% - 80\%, C). \tag{31}$$

4.2.2. Parameter sensitivity under real-world driving cycles

Unlike the pioneering work [10,11] only using constant C-rate discharging profiles to investigate the parameter sensitivity, we applied a battery current profile generated by an EV model [37] under a repeated Worldwide harmonized Light vehicle Test Procedure (WLTP), as shown in Fig. 2. Thus, it can provide us the sensitivity of the parameters in an electrochemical model-based BMS under the real operation load of EVs.

Similarly, the mean standard deviation of the analyzed state x_i in the whole time domain was chosen as SI,

$$SI = \frac{1}{N_t}\sum_{i=1}^{N_t}\sqrt{\frac{1}{N_s}\sum_{j=1}^{N_s}(x_{ij} - \bar{x}_i)^2} \tag{32}$$

where N_t is the number of data points in the time domain in each simulation and $\bar{x}_i$ is the average value of the states x_{ij}.

5. Results and discussion

5.1. Parameter sensitivity under constant C-rate charging process

A total of 3640 CC-CV charging experiments were simulated with our reduced-order electrochemical model in MATLAB. The influences of C-rate and DOD regions on the parameter sensitivity were investigated based on these CC-CV charging experiments.

First of all, we have observed different influences of C-rate and DOD regions on capacity-related parameters and other parameters. In order to provide insight into this phenomenon, we depict the simulation results of a capacity-related parameter, anode active material volume fraction ε_s^+, and a parameter which is not related to capacity, anode particle radius R_p^-, under 1 C and 5 C charging in Fig. 3. The terminal voltage shows significant voltage variations in all depicted simulations and is therefore sensitive to both parameters. Yet, these two parameter sensitivities are differently dependent on C-rate and DOD regions. With the increase of C-rate from 1 C to 5 C, the sensitivity of R_p^- increased significantly while the sensitivity of ε_s^+ has no significant change. Furthermore, the variance of ε_s^+ results in the horizontal shift of the end-of-charge point, which brings the difference of the ASI in low DOD regions. In contrast, the variance of R_p^- results in the vertical shift of the whole terminal voltage curve, which increases the sensitivity of R_p^- in all DOD regions.

To further understand the reason behind this difference, sensitivity matrices were generated for all 26 analyzed parameters, where each matrix contains 35 sensitivity elements (five DOD regions with seven C-rates) calculated by the method introduced in Section 4.2.1. In order to assess the influence of C-rate and DOD regions for all the parameters, the sensitivity matrix for each parameter was normalized between zero and one and visualized in Fig. 4. Each point indicates the normalized SI under a certain DOD region and C-rate. The larger the scatter point is, the higher the sensitivity of the parameter under that experimental condition is. It is clear that the sensitivity of seven parameters, i.e., L^+, L^-, ε_s^+, ε_s^-, $c_{s,\max}^+$, $c_{s,\max}^-$ and A, vary significantly at different DOD regions, while the variations caused by the increase of C-rate are moderate. In particular, all these seven parameters have an influence on the capacity, as the capacity of the cell can be defined as,

$$Q = \frac{A\varepsilon_s^+ L^+ c_{s,max}^+ F|\theta_{100}^+ - \theta_0^+|}{3600} = \frac{A\varepsilon_s^- F L^- c_{s,max}^- F|\theta_{100}^- - \theta_0^-|}{3600}. \tag{33}$$

Therefore, the variation of these parameters has a strong impact on the cell capacity, which leads to the horizontal shift of the end-of-charge point, as observed in Fig. 3a and 3b. Hence, a significant variance of parameter sensitivity under different DOD regions can be observed.

In contrast, a significant increase of sensitivity was observed with an increase of the C-rate for all the rest 19 parameters, which are not related to cell capacity. However, the difference in the parameter sensitivity among five DOD regions is small, as observed in Fig. 3c and 3d. This indicates that the increase in C-rate will increase the identifiability of these 19 parameters in the whole DOD range during the data-based parameter identification process.

5.2. Parameter sensitivity under real-world driving cycles

Apart from the CC-CV experiments, 260 WLTP experiments were simulated with our reduced-order electrochemical model. To further provide insight into the parameter sensitivity under real-world driving cycles, simulation results under the WLTP for the sensitivity analysis of cathode active material volume fraction ε_s^+ are shown in Fig. 5. During the simulation, ε_s^+ was increasing from 0.35 to 0.5 step by step. As ε_s^+ is a capacity-related parameter, a similar phenomenon, as depicted in Fig. 3a and b, was observed not only for the terminal voltage but also for cathode bulk SOC and surface SOC, as shown in Fig. 5a, b, and c. With the increase of ε_s^+, the capacity of the battery increases and reduces the change of SOCs and terminal voltage with the same discharged capacity. Therefore, the terminal voltage, cathode bulk SOC, and cathode surface SOC are sensitive for the variation of ε_s^+. In contrast, no significant change of the anode potential Φ^- can be observed, as shown in Fig. 5d, which indicates the insensitivity of ε_s^+ for Φ^-.

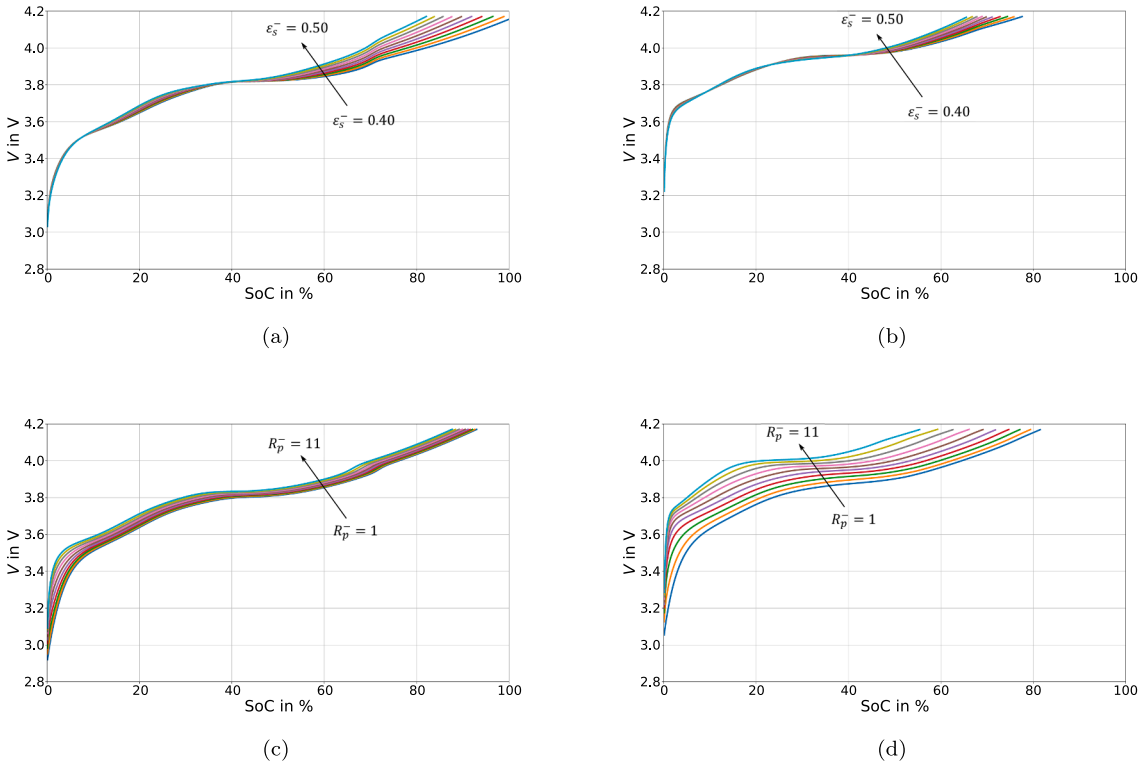

Fig. 3. Comparison of the sensitivity analysis results between capacity-related parameters and other parameters under the charging process with different C-rates. (a) Results of ε_s^+ under 1 C charging. (b) Results of ε_s^- under 5 C charging. (c) Results of R_p^- under 1 C charging. (d) Results of R_p^- under 5 C charging.

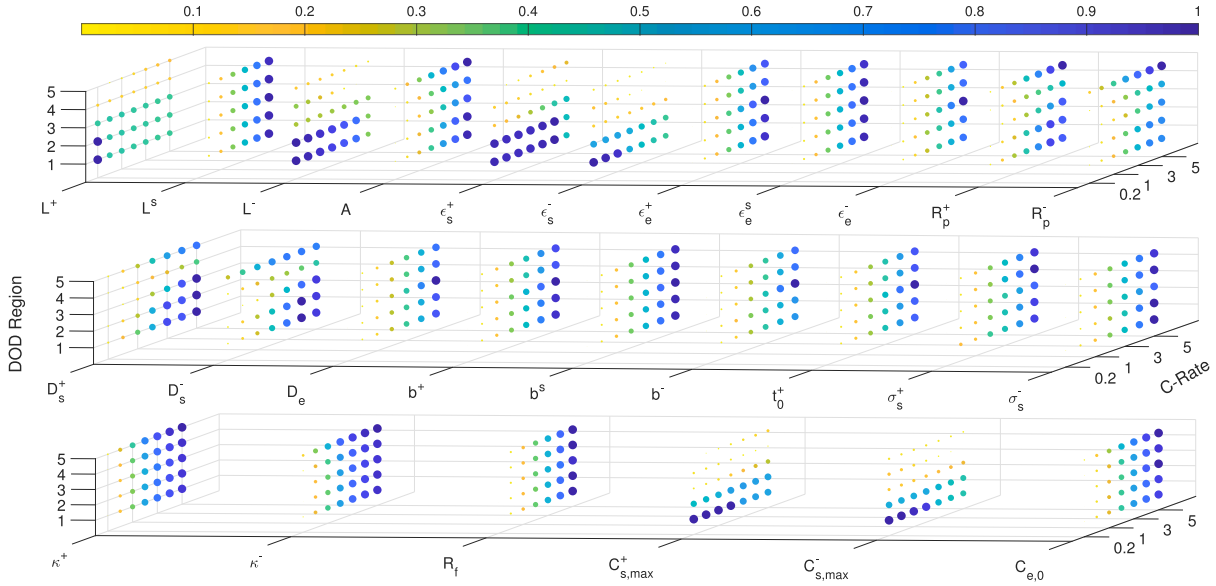

Fig. 4. Normalized sensitivity matrices for 26 physical parameters under seven different C-rates and five different DOD regions. The parameters are categorized into three rows: geometric parameters, transport parameters, kinetic and concentration parameters.

One of the goals of this work is to analyze the identifiability of the parameters based on terminal voltage measurement data. The ranking of the normalized SI of all the 26 parameters for the terminal voltage is shown in Fig. 6. Out of 26 parameters, 14 parameters with the value of normalized SI greater than 0.01 are defined as sensitive parameters for the terminal voltage. The identification of these parameters based on the terminal voltage data under WLTP profile with global optimization algorithms, e.g., genetic algorithm [38], will be relatively accurate. A fast data-based identification of these parameters can not only improve the parameter accuracy compared with experimental methods but also greatly reduce the time and equipment cost.

Besides, all the cell capacity-related parameters, e.g., electrode thickness $L^{\pm}$, electrode surface area A, active material volume fraction $\varepsilon_s^{\pm}$ and maximum electrode ionic concentration $c_{s,max}^{\pm}$ as shown in (33), have a very high sensitivity for the terminal voltage.

Considering that the state-of-the-art experimental parameter identification method can generate relatively large measurement error, accurate identification of these parameters with data-based methods will help ensure the good operation of an electrochemical model-based BMS. Furthermore, data-based parameter identification methods can

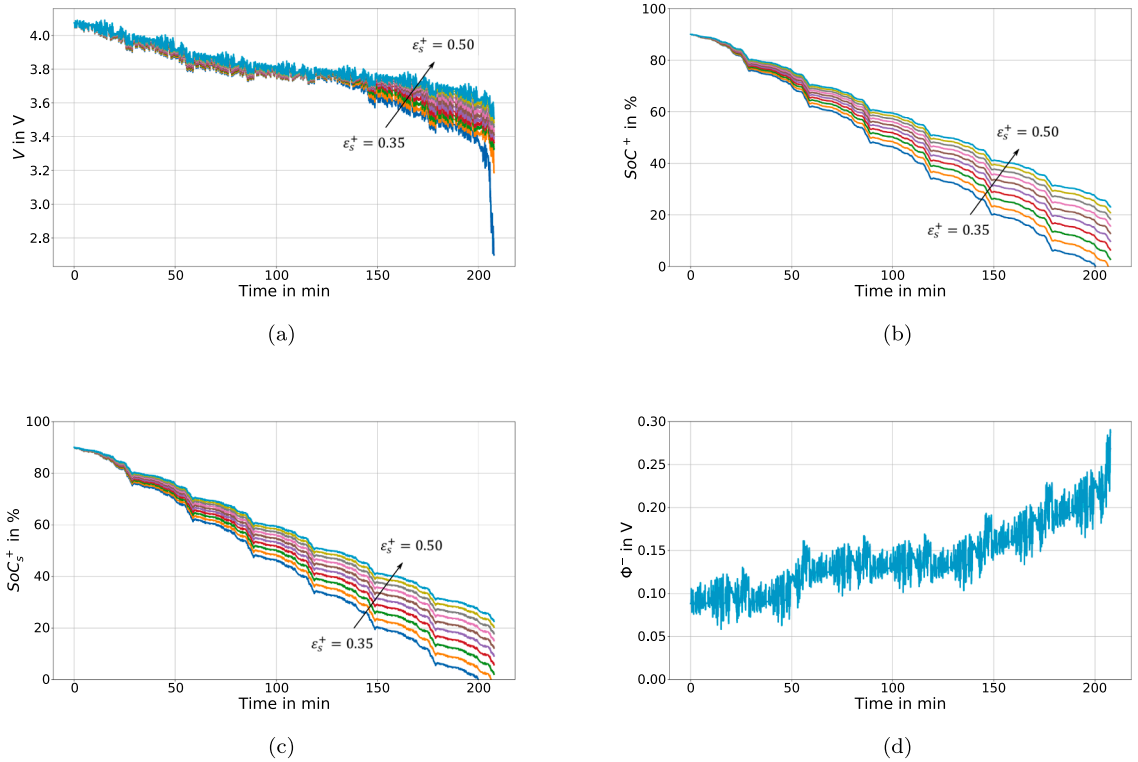

Fig. 5. Comparison of sensitivity analysis results for cathode active material volume fraction ε_s^+ among essential BMS states. (a) Results of ε_s^+ for terminal voltage. (b) Results of ε_s^+ for cathode bulk SOC. (c) Results of ε_s^+ for cathode surface SOC. (d) Results of ε_s^+ for anode potential.

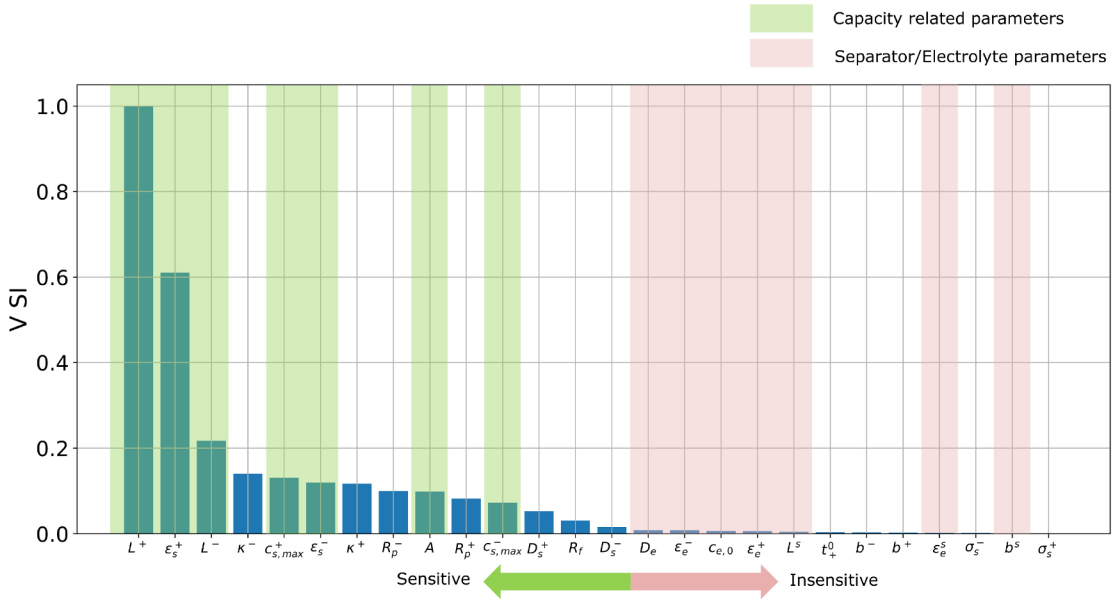

Fig. 6. Ranking of the normalized parameter sensitivity for terminal voltage under real-world driving cycles.

also provide rich information about the electrode-level capacity degradation mechanisms of LIBs during aging, e.g., lithium-ion loss and active material loss.

Apart from 14 sensitive parameters, there are also 12 insensitive parameters in the electrochemical model, which means the accuracy of the identification of these parameters will be relatively low. Therefore, it is important to investigate the influence of the inaccuracy of these insensitive parameters on the functionalities of the electrochemical model-based BMS. To this end, the normalized SI values of parameters were calculated for each BMS state and grouped in categories, as shown in Fig. 7.

The sensitivity rankings change dramatically with different BMS states. The sensitive parameters for cathode surface SOC and bulk SOC are cathode parameters and the sensitive parameters for anode potential are anode parameters. Furthermore, it is found that all 12 insensitive parameters for the terminal voltage are also insensitive for the other BMS states, no matter in cathode or anode. Thus, the inaccurate identification of these parameters has little influence on the operation of BMS functionalities.

It is also worth noting that all of the separator parameters and electrolyte parameters are insensitive for this cell. Except for the solid diffusion coefficients $D_s^{\pm}$, all the transport parameters are also insensitive for BMS states. However, one should not expect these conclusions to be generally true across all cell chemistries.

6. Conclusions

The sensitivity of 26 physical parameters of a lithium-ion electrochemical model was analyzed for lithium-NMC-graphite battery cells in this work. The study was conducted not only under constant C-rate

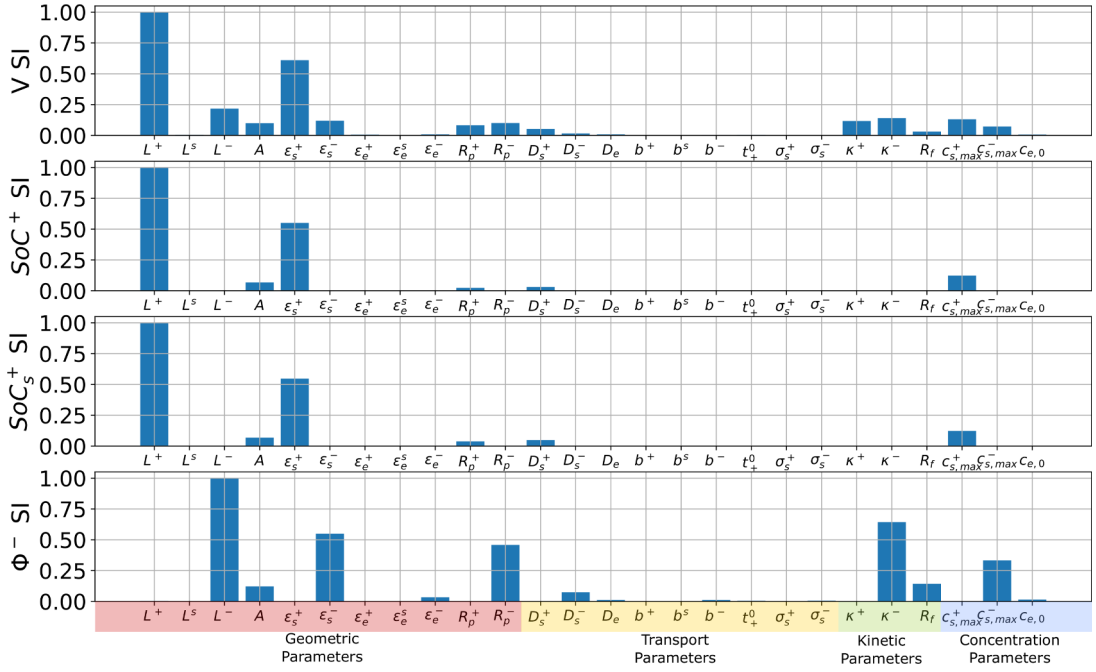

Fig. 7. Rankings of the normalized parameter sensitivity for terminal voltage, cathode bulk SOC, cathode surface SOC and anode potential.

charging process but also under real-world driving cycles of EVs. The main conclusions of this work are summarized as follows:

- All seven capacity-related parameters have shown significant sensitivity variance for the terminal voltage in different DOD regions, which is caused by the horizontal shift of the end-of-charge point due to the capacity change. In contrast, the variance of the rest 19 parameters results in the vertical shift of the whole terminal voltage curve, where the variance among DOD regions is small.
- The sensitivity of 19 parameters, which are not related to the cell capacity, can be increased significantly by increasing the C-rate. This indicates the possibility to increase the identifiability of these parameters by using large C-rate current in experiments. In contrast, similar effects have not been observed for seven capacity-related parameters.
- Apart from using constant C-rate charging profiles, a battery current profile generated by an EV model under a repeated WLTP driving cycle was applied for the first time to investigate the parameter sensitivity for the electrochemical model-based BMS. According to the sensitivity rankings of the parameters, 14 parameters are sensitive for terminal voltage and can be identified with acceptable accuracy based on the terminal voltage measurement data. Furthermore, all seven capacity-related parameters have relatively high sensitivity for the terminal voltage. The identification of these parameters will provide rich information on electrode level capacity degradation mechanisms.
- The sensitivity of all 26 physical parameters was analyzed not only for the terminal voltage but also for the essential states in an electrochemical model-based BMS, e.g., cathode bulk state of charge, cathode surface state of charge and anode potential. Among 26 parameters, 12 parameters are insensitive for the terminal voltage, containing all the separator and electrolyte parameters. However, they are all insensitive for other essential BMS states, which means the influence of inaccuracy of these parameters on the functionalities of the BMS is low. We believe that this is the first work that shows the influence of the inaccuracy of parameter identification on the main functionalities in an electrochemical model-based BMS.
- The contribution of this work for the development of BMSs can be summarized as follows. First, the focus of the parameter identification function in BMSs should be on the 14 sensitive parameters, the accuracy of which is crucial for the main BMS functionalities. Second, sensitive parameters are defined individually for state of energy, state of power and fast charging, which should be considered during the development of these functionalities. At last, the provided information on the parameter sensitivity under real-world driving cycles give us inspiration on the design of online parameter identification algorithms in BMSs.

The conclusions in this work are based on the 7.5 Ah Kokam SLCB cells with NMC and graphite as cathode and anode material, respectively. In future work, the universality of the results will be checked for the battery cells with other materials, such as $LiFePO_4$/*graphite* cells, and under other current loads. Furthermore, a fast parameter identification framework for electrochemical model-based BMS will be designed and validated for real lithium-NMC-graphite battery cells based on the sensitivity analysis results in this work. Compared with the state-of-the-art experimental or data-based parameter identification methods, this new identification framework will further reduce the time consumption and increase identification accuracy.

CRediT authorship contribution statement

Weihan Li: Conceptualization, Methodology, Software, Validation, Investigation, Writing - original draft, Writing - review & editing, Visualization. **Decheng Cao:** Software, Validation, Writing - original draft, Visualization. **Dominik Jöst:** Resources, Writing - review & editing. **Florian Ringbeck:** Resources, Writing - review & editing. **Matthias Kuipers:** Resources, Writing - review & editing. **Fabian Frie:** Writing - review & editing. **Dirk Uwe Sauer:** Conceptualization, Writing - review & editing, Supervision, Funding acquisition.

Declaration of Competing Interest

The authors declare that they have no known competing financial interests or personal relationships that could have appeared to influence the work reported in this paper.

Acknowledgment

This work was financially supported within the project EVERLASTING from the Horizon 2020 program by the European Union [Grant No. EVERLASTING-713771]. The authors gratefully acknowledge the support by RWTH Aachen University with the computing resources under the project thes0564.

References

[1] Stuart T, Fang F, Wang X, Ashtiani C, Pesaran A. A modular battery management system for hevs. In: SAE Technical Paper Series, SAE Technical Paper Series. 400 Commonwealth Drive, Warrendale, PA, United States: SAE International; 2002. doi:10.4271/2002-01-1918.
[2] Chaturvedi NA, Klein R, Christensen J, Ahmed J, Kojic A. Algorithms for advanced battery-management systems. IEEE Control Syst 2010;30(3):49–68. https://doi.org/10.1109/MCS.2010.936293.
[3] Ecker M, Tran TKD, Dechent P, Käbitz S, Warnecke A, Sauer DU. Parameterization of a physico-chemical model of a lithium-ion battery: Part I. Determination of parameters. J Electrochem Soc 2015;162(9):A1836–48. https://doi.org/10.1149/2.0551509jes.
[4] Ecker M, Käbitz S, Laresgoiti I, Sauer DU. Parameterization of a physico-chemical model of a lithium-ion battery: Part II. Model validation. J Electrochem Soc 2015;162(9):A1849–57. https://doi.org/10.1149/2.0541509jes.
[5] Schmalstieg J, Rahe C, Ecker M, Sauer DU. Full cell parameterization of a high-power lithium-ion battery for a physico-chemical model: Part I. Physical and electrochemical parameters. J Electrochem Soc 2018;165(16):A3799–810. https://doi.org/10.1149/2.0321816jes.
[6] Schmalstieg J, Sauer DU. Full cell parameterization of a high-power lithium-ion battery for a physico-chemical model: Part II. Thermal parameters and validation. J Electrochem Soc 2018;165(16):A3811–9. https://doi.org/10.1149/2.0331816jes.
[7] Tang S, Wang Z, Guo H, Wang J, Li X, Yan G. Systematic parameter acquisition method for electrochemical model of 4.35 v licoo2 batteries. Solid State Ionics 2019;343:115083. https://doi.org/10.1016/j.ssi.2019.115083.
[8] Schmidt AP, Bitzer M, Imre ÁW, Guzzella L. Experiment-driven electrochemical modeling and systematic parameterization for a lithium-ion battery cell. J Power Sources 2010;195(15):5071–80. https://doi.org/10.1016/j.jpowsour.2010.02.029.
[9] Forman JC, Moura SJ, Stein JL, Fathy HK. Genetic identification and fisher identifiability analysis of the doyle–fuller–newman model from experimental cycling of a lifepo4 cell. J Power Sources 2012;210:263–75. https://doi.org/10.1016/j.jpowsour.2012.03.009.
[10] Zhang L, Lyu C, Hinds G, Wang L, Luo W, Zheng J, et al. Parameter sensitivity analysis of cylindrical lifepo 4 battery performance using multi-physics modeling. J Electrochem Soc 2014;161(5):A762–76. https://doi.org/10.1149/2.048405jes.
[11] Edouard C, Petit M, Forgez C, Bernard J, Revel R. Parameter sensitivity analysis of a simplified electrochemical and thermal model for li-ion batteries aging. J Power Sources 2016;325:482–94. https://doi.org/10.1016/j.jpowsour.2016.06.030.
[12] Ghaznavi M, Chen P. Sensitivity analysis of a mathematical model of lithium–sulfur cells part i: Applied discharge current and cathode conductivity. J Power Sources 2014;257:394–401. https://doi.org/10.1016/j.jpowsour.2013.10.135.
[13] Doyle M, Fuller TF, Newman J. Modeling of galvanostatic charge and discharge of the lithium/polymer/insertion cell. J Electrochem Soc 1993;140(6):1526. https://doi.org/10.1149/1.2221597.
[14] Subramanian VR, Boovaragavan V, Ramadesigan V, Arabandi M. Mathematical model reformulation for lithium-ion battery simulations: Galvanostatic boundary conditions. J Electrochem Soc 2009;156(4):A260. https://doi.org/10.1149/1.3065083.
[15] Cai L, White RE. Reduction of model order based on proper orthogonal decomposition for lithium-ion battery simulations. J Electrochem Soc 2009;156(3):A154. https://doi.org/10.1149/1.3049347.
[16] Ringbeck F, Li W, Garbade M, Sauer DU. Critical review of electrochemical model-based battery management system: modelling and model order reduction (in process). J Power Sources.
[17] Erhard Sv, Osswald PJ, Keil P, Höffer E, Haug M, Noel A, et al. Simulation and measurement of the current density distribution in lithium-ion batteries by a multi-tab cell approach. J Electrochem Soc 2017;164(1):A6324–33. https://doi.org/10.1149/2.0551701jes.
[18] Smith K, Wang C-Y. Solid-state diffusion limitations on pulse operation of a lithium

ion cell for hybrid electric vehicles. J Power Sources 2006;161(1):628–39. https://doi.org/10.1016/j.jpowsour.2006.03.050.
[19] Ji Y, Zhang Y, Wang C-Y. Li-ion cell operation at low temperatures. J Electrochem Soc 2013;160(4):A636–49. https://doi.org/10.1149/2.047304jes.
[20] Smekens J, Paulsen J, Yang W, Omar N, Deconinck J, Hubin A, et al. A modified multiphysics model for lithium-ion batteries with a lixni1/3mn1/3co1/3o2 electrode. Electrochim Acta 2015;174:615–24. https://doi.org/10.1016/j.electacta.2015.06.015.
[21] Stewart SG, Srinivasan V, Newman J. Modeling the performance of lithium-ion batteries and capacitors during hybrid-electric-vehicle operation. J Electrochem Soc 2008;155(9):A664. https://doi.org/10.1149/1.2953524.
[22] Rheinfeld A, Sturm J, Noel A, Wilhelm J, Kriston A, Pfrang A, et al. Quasi-isothermal external short circuit tests applied to lithium-ion cells: Part ii. modeling and simulation. J Electrochem Soc 2019;166(2):A151–77. https://doi.org/10.1149/2.0071902jes.
[23] Nileshwar PR, McGordon A, Ashwin TR. Greenwood, Parametric optimization study of a lithium-ion cell. Energy Procedia 2017;138:829–34. https://doi.org/10.1016/j.egypro.2017.10.088.
[24] Fang W, Kwon OJ, Wang C-Y. Electrochemical-thermal modeling of automotive li-ion batteries and experimental validation using a three-electrode cell. Int J Energy Res 2010;34(2):107–15. https://doi.org/10.1002/er.1652.
[25] Lee H, Yanilmaz M, Toprakci O, Fu K, Zhang X. A review of recent developments in membrane separators for rechargeable lithium-ion batteries. Energy Environ Sci 2014;7(12):3857–86. https://doi.org/10.1039/C4EE01432D.
[26] Tanim TR, Rahn Cd, Wang C-Y. A temperature dependent, single particle, lithium ion cell model including electrolyte diffusion. J Dyn Syst Meas Contr 2015;137(1):011005. https://doi.org/10.1115/1.4028154.
[27] Awarke A, Pischinger S, Ogrzewalla J. Pseudo 3d modeling and analysis of the sei growth distribution in large format li-ion polymer pouch cells. J Electrochem Soc 2013;160(1):A172–81. https://doi.org/10.1149/2.022302jes.
[28] Capiglia C, Saito Y, Kageyama H, Mustarelli P, Iwamoto T, Tabuchi T, et al. 7li and 19f diffusion coefficients and thermal properties of non-aqueous electrolyte solutions for rechargeable lithium batteries. J Power Sources 1999;81–82:859–62. https://doi.org/10.1016/S0378-7753(98)00237-7.
[29] Ehrl A, Landesfeind J, Wall WA, Gasteiger HA. Determination of transport parameters in liquid binary lithium ion battery electrolytes. J Electrochem Soc 2017;164(4):A826–36. https://doi.org/10.1149/2.1131704jes.
[30] Nyman A, Behm M, Lindbergh G. Electrochemical characterisation and modelling of the mass transport phenomena in lipf6–ec–emc electrolyte. Electrochim Acta 2008;53(22):6356–65. https://doi.org/10.1016/j.electacta.2008.04.023.
[31] Valoen LO, Reimers JN. Transport properties of lipf[sub 6]-based li-ion battery electrolytes. J Electrochem Soc 2005;152(5):A882. https://doi.org/10.1149/1.1872737.
[32] Chen Y-H, Wang C-W, Zhang X, Sastry AM. Porous cathode optimization for lithium cells: Ionic and electronic conductivity, capacity, and selection of materials. J Power Sources 2010;195(9):2851–62. https://doi.org/10.1016/j.jpowsour.2009.11.044.
[33] Park M, Zhang X, Chung M, Less GB, Sastry AM. A review of conduction phenomena in li-ion batteries. J Power Sources 2010;195(24):7904–29. https://doi.org/10.1016/j.jpowsour.2010.06.060.
[34] Uhlmann C, Illig J, Ender M, Schuster R, Ivers-Tiffée E. In situ detection of lithium metal plating on graphite in experimental cells. J Power Sources 2015;279:428–38. https://doi.org/10.1016/j.jpowsour.2015.01.046.
[35] Legrand N, Knosp B, Desprez P, Lapicque F, Raël S. Physical characterization of the charging process of a li-ion battery and prediction of li plating by electrochemical modelling. J Power Sources 2014;245:208–16. https://doi.org/10.1016/j.jpowsour.2013.06.130.
[36] Song M, Choe S-Y. Fast and safe charging method suppressing side reaction and lithium deposition reaction in lithium ion battery. J Power Sources 2019;436:226835. https://doi.org/10.1016/j.jpowsour.2019.226835.
[37] Nemeth T, Bubert A, Becker JN, de Doncker RW, Sauer DU. A simulation platform for optimization of electric vehicles with modular drivetrain topologies. IEEE Trans Transp Electrif 2018;4(4):888–900. https://doi.org/10.1109/TTE.2018.2869371.
[38] Whitley D. A genetic algorithm tutorial. Stat Comput 4(2). doi: 10.1007/BF00175354.